JST: Engineering and Technology for Sustainable Development
Volume 35, Issue 2, April 2025, 049-057

Effect of Grain Size on the Mechanical Properties of Compositionally Graded Copper-Nickel Nanocrystalline: a Molecular Dynamic Simulation Study

Dang Thi Hong Hue*, Doan Minh Quan
Hanoi University of Science and Technology, Ha Noi, Vietnam
**Corresponding author email: hue.dangthihong@hust.edu.vn*

Abstract

The mechanical properties of compositionally graded nanocrystalline materials (CGNMs) are studied via molecular dynamics simulation. However, achieving a complete understanding of the mechanical behavior of CGNMs with different grain sizes, particularly at the atomic level, has remained elusive. This article uses molecular dynamics (MD) simulations to investigate the tensile mechanical properties of CuNi CGNMs with varying grain sizes. The findings demonstrate that the yielding stress of CGNMs increases with a decrease in the grain sizes. Research shows that the critical value of the average grain diameter available to transform the positive Hall-Petch relationship to an inverse one is d_c equals 11.09 nm; at this size, the largest yield strength (YS) is 2.7 GPa. This is explained as the average grain diameter has not reached the critical value, the dislocations move during plastic deformation, and they accumulate at grain boundaries to form dislocation clusters that prevent the further movement of other dislocations. This phenomenon causes the materials to strengthen. When the grain size is smaller than the critical value, the grain volume is too small to contain enough dislocations. Therefore, dislocations gliding across the boundary quickly reduce the YS, which means materials soften due to the rotation or gliding of grain boundaries. This change in YS is consistent with the inverse Hall-Petch relationship.

Keywords: Compositionally graded nanocrystalline materials, mechanical properties, grain size, molecular dynamics simulation.

1. Introduction

Compositionally graded nanocrystalline materials (CGNMs) are the most promising among many advanced materials. They consist of two or more elements where the composition continuously varies along a dimension following a particular function [1]. Compositionally graded nanocrystalline materials are conceived solutions to solve high-stress concentration, high-temperature creep, and material delamination challenges common in other fabricated materials such as composites. These enhanced thermal and mechanical properties render CGNMs a suitable candidate for manufacturing structures of airplanes, automobile engine components, and protective coatings for turbine blades.

However, CGNMs also exhibit some distinct properties compared to homogeneous metals and alloys, such as mechanical properties that are not stable in regions with variable composition. Especially, the characteristics of CGNMs depend not only on their compositions but also on the grain size. Based on this characteristic, designing the CGNMs according to the predetermined component will produce the material with the desired mechanical properties. Therefore, a thorough explanation of the correlation between the grain size of CGNMs and their mechanical properties is essential and significant for the investigation, design, and use of materials.

Two major approaches have been employed in material fabrication: top-down and bottom-up. Mechanical methods, such as rolling and forging, are a top-down approach used primarily to change the composition of the material's surface. This method produces a multi-layer variable material with a thickness of less than 10 nm per layer. Besides, the second bottom-up approach includes chemical, physical, electroplating, sputtering, laser firing, and metal 3D printing techniques. These techniques allow the production of thin films or sheets with thicknesses greater than 10 nm up to several hundred nm. The laws of composition and materials used when manufacturing are diverse and follow the rules. Many studies have been conducted to evaluate the mechanical properties of CGNMs. Steel materials have been successfully synthesized with variable compositions, and it was observed that a decrease in chemical stability and forming a ferrite layer in these materials significantly increases the destructive

ISSN 2734-9381
https://doi.org/10.51316/jst.181.etsd.2025.35.2.7
Received: Aug 30, 2024; revised: Oct 1, 2024
accepted: Oct 15, 2024

strength, increasing the material's toughness. It was suggested that the component gradient in Fe-C steel, made by partial decarbonization, can reduce the rate of durable chemistry resulting in increased strength for the material. Studies about the variable materials of Mo/Al for an exponential symmetry sample with different exponential values have concluded that the strength of the material depends so much on the exponential value. The internal crack position in CGNMs relies on the direction of composition change.

Beyond empirical research, theoretical studies of the CGNMs have also been conducted using the theory of continuum environmental mechanics. In particular, Karman's theory has been applied to analyze large deformations of material plates that vary under transverse forces [2]. Furthermore, the finite element method has been used to study the deformation of variable materials under the action of shear loads. Another study has focused on the effect of radial loads on the mechanical behavior of CGNMs. However, these studies did not consider the effects of microstructure, interactions between atoms, dislocations, and planar defects on the mechanical behavior of CGNMs at the nanoscale. Therefore, this study must demonstrate the influence of all the above factors on the mechanical properties and behavior of CGNMs in atomic-level detail.

Recent studies have used molecular dynamics (MD) simulations to clarify the mechanical behavior of CGNMs, demonstrating that materials can change mechanical properties by changing material composition [3]. MD simulation proved to be a suitable approach for studying the mechanical properties of nanostructured CGNMs. However, some important issues related to the mechanical behavior of CGNMs remain unresolved, such as the mechanism behind changes in the degree of deformation of materials, the formation and development of deviations, stacking errors, and the influence of CGNMs at the nanoscale. Addressing these research questions will continue to advance studies of the mechanical properties of CGNMs.

The literature review does not provide any published research on the influence of grain size on the mechanical properties of CGNMs, so this research could partly fill this gap. In this study, the mechanics of CGNMs subjected to tension are investigated using MD simulations. The effect of grain size on the mechanical properties is investigated by considering different grains that govern the composition distribution profiles of CGNMs. Various mechanical properties, including Young's modulus (YM), yielding stress (YS), and ultimate tensile strength (UTS), are evaluated and compared among the different grain sizes.

2. Method

2.1. Simulation Model

This study analyzes the mechanical properties of CGNMs characterized by different grain sizes through MD simulations. We selected compositionally graded nanocrystalline materials of Cu and Ni elements due to extraordinary immunity to seawater corrosion. In particular, CuNi alloys are resistant to chlorides in terms of pitting, cracking due to stress corrosion, and even in hotter climates. Both elements are widely used because of their exceptional electronic, magnetic, and catalytic properties. Cu–Ni alloy nanostructures reveal advantageous properties such as good electronic conductivity, brilliant magnetism, and favorable chemical stability, which could find probable applications in nano-electronics. Moreover, these alloys show high tensile, compressive, and bending strength. They are also commonly used for manufacturing various components in the oil, marine, and chemical industries, such as pumps, impellers, drill collars, valves, pipes, and propeller shafts of marine and submarine engines [4]. At below 1358K, at all alloying percentages, Cu–Ni forms only a single α-phase and Ni atoms supernumerary Cu atoms randomly from copper's FCC lattice points in α-phase. Several studies on the properties of alloys and modified materials of these two elements have been used by some authors to study their mechanical properties [5]. Due to the reasons above, we have chosen Ni and Cu as the alloying constituents of CGNMs.

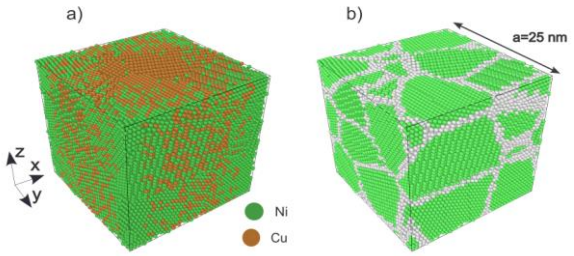

Fig. 1. Schematic illustration of CuNi CGNMs. (a) Atomic rearrangements of CGNMs (b) Distribution of grains, with white atoms are on the boundaries.

The cuboid simulation boxes are the same size $a \times a \times a$ = 25 nm × 25 nm × 25 nm as shown in Fig 1. Each simulation box has a different number of grains. Table 1 shows the average diameter of a grain d and its roof square d.

Note that recent advances in nanomaterial fabrication techniques have allowed us to create nanowires with a diameter of about 5 nm. The nanowire size used in the current study matches the size that can be made experimentally [6].

Table 1. Grains information

Grain numbers(*n*)	***d***(nm)	**1/ $d^{1/2}$**$(nm)^{1/2}$
5	14.85	0.26
7	13.28	0.27
9	12.21	0.29
12	11.09	0.30
14	10.54	0.31
18	9.69	0.32
25	8.69	0.34
30	8.17	0.35

The Descartes coordinate system is used with the crystal directions [100], [010] and [001] aligned along the *x*, *y*, and *z* directions respectively. The {100} system of the basal umbrella is similar to that found in experimental studies. For example, different research groups have successfully synthesized Cu-nanowires with the {100}. Therefore, the CGNMs used in our research have surfaces {100} closely resemble those achieved in experiments. An important determinant of the properties of compositionally graded nanomaterials is the classification function. In the case of CGNMs, the energy law function is mainly used.

This study uses energy law relationships to govern the composition variation of CGNMs, in which Cu and Ni atoms align themselves in a face-centered cubic lattice (FCC) structure. The mathematical expression for the change of Ni content in CGNMs is indicated as [7]:

$$g(r) = \left(\frac{r}{R}\right)^p \tag{1}$$

where f is the mass fraction of the component Ni, and *p* is the exponent of the gradient index. The dependence of the Ni distribution on the gradient index of CGNMs is illustrated with $p = 1$ made in this study.

The lattice constants of Cu (a_{Cu}) and Ni (a_{Ni}) at 0K are 3.6 Å and 3.52 Å, respectively, which induces the lattice misfit between Cu and Ni of approximately 2.2%. We use an average lattice constant of the Cu and Ni equals $(a_{Cu} + a_{Ni})/2$ is 3.56 Å to build CuNi CGNMs models. This approach applies to CGNMs where the lattice misfit between the constituents is moderate or small, such as Cu-Ni, Ti-Al, and Ag-Au alloys [8]. The process of constructing a CG-NW involves 3 steps. Firstly, a pure Cu nanowires is generated with an FCC structure and lattice constant of 3.56 Å. Secondly, the Cu nanowires are divided into portions along the *z*-direction, each with a length of 3.6. Finally, Cu atoms within each portion are substituted by Ni atoms, with the mass fraction determined by (1). Additionally, the length of the CGNWs is significantly larger than the length of each portion, resulting in a smooth composition gradient that can be considered as a continuous variation.

2.2. Interatomic Potential and Simulation Procedure

The embedded-atom method (EAM) potential is employed to model the pairwise interactions of Cu and Ni elements. This approach is commonly used for metallic and intermetallic compounds. The total energy of the system denoted as ETotal, comprising N atoms, can be expressed as follows [9]:

$$E_{\text{Total}} = \sum_{i=1}^{N} (F_i(\rho_i) + \frac{1}{2}\sum_{j \neq i} \phi_{ij}(r_{ij}) \tag{2}$$

$$\rho_i = \sum_{j \neq i} \rho_{ij}^a(r_{ij}) \tag{3}$$

where F_i represents the embedding energy of atom *i*, ρ_i corresponds to the electron density at site *i*, ϕ_{ij} denotes the pair potential function between atoms *i* and *j*, and ρ_{ij}^a is the atomic charge density of atom *j* at the location of atom *i*. MD simulations are performed using the LAMMPS package [10]. Verlet's numerical integration algorithm is applied to estimate the position and velocity of atoms. A Nose-Hoover thermostat is used to maintain a temperature of 300 K, while the Berendsen barostat is employed to stabilize the system's pressure at 0 bar. The time step is set to 0.001ps, the damping parameter is 0.1, and the drag factors of the thermostat are adjusted to 1.0. After conducting preliminary simulations and carefully analyzing the behavior of total energy and atomic oscillation, a relaxation time of 50 ps is selected. Periodic boundary conditions are imposed in the loading direction, while the simulation domain boundaries in the *x* and *y* directions are non-periodic and shrink-wrapped. Before the tensile test simulations, a conjugate gradient minimization scheme minimizes the system's energy. Afterward, simulations are conducted using the NPT (fixed number of particles *(N)*, temperature *(T)*, and pressure (P) to achieve thermal equilibration. The NVE (fixed number of particles *(N)*, volume *(V)*, and average energy content *(E)* ensembles for a duration of 100 ps were employed [11]. Once the CGNMs reach an equilibrium state, a uniaxial strain along the *z*-direction is applied to the CGNMs with a strain rate of 10^{10} s^{-1} and a maximum value of 30 %. This process allows for the exploration of their mechanical behavior. In MD simulations, strain rates ranging from 10^9 s^{-1} to 10^{10} s^{-1} are commonly employed to investigate the mechanical properties of materials. We used a strain rate of 10^{10} s^{-1} due to computational limitations in this investigation.

2.3. Analysis Methods

Three analysis methods are used to identify the microstructure evolution, including centrosymmetry parameter (CSP) analysis, common neighbor analysis (CNA), and dislocation extraction analysis (DXA). The CSP analysis is different structures based on the CSP, which measures the local lattice disorder around an atom from a perfect lattice. The CNA is employed for locating dislocation cores and also stacking faults Finally, the DXA separates the crystal into good and bad crystal regions using the common neighbor analysis method. On the other hand, atomic-level stress tensors are following equation:

$$\sigma_{\alpha\beta}(i) = -\frac{1}{2\Omega}\left(\sum_j F_{ij}^{\alpha} r_{ij}^{\beta} + 2M_i v_i^{\alpha} v_i^{\beta}\right) \quad (4)$$

where α and β denote the Cartesian components; Ω is the atomic volume; F_{ij} is the force on atom i due to atom j; M_i is the mass of atom i, and vi is the velocity of atom i. The atomic arrangements and evolution of microstructures are visualized and obtained with OVITO software [12].

3. Results and Discussion

3.1. Mechanical Properties of Polycrystalline Compositionally Graded Nanomaterials

Mechanical behaviors of CGNMs under uniaxial tensile tests with different grain sizes are represented in Fig. 2. The strain increases linearly with the stress increase until a value of 4 % is reached. This shows that with a small strain, there is no plastic deformation in CGNMs, when the strain is larger than 0.02, the stress-strain curves depart from each other. With a strain greater than 4%, the stress increases nonlinearly until it reaches the peak of stress (UTS) at a fracture strain of 6%, and the stress sharply drops (strain softening). The behavior of CGNMs is similar to ductile materials of Ni or Cu.

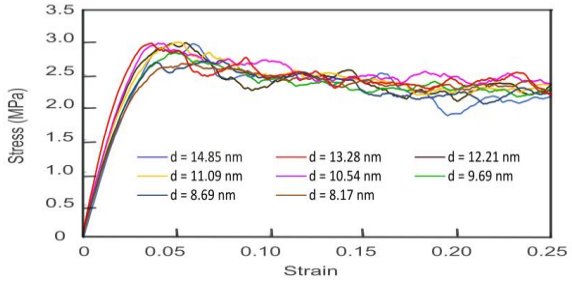

Fig. 2. Stress-strain curves of CGNMs with different grain sizes

To gain a deeper understanding of the mechanical properties of CGNMs with various grain sizes, the ultimate tensile strength (UTS) is considered first. The UTS significantly depends on the grain sizes in Fig. 3. It is obvious that the UTS increases with the decreasing grain sizes if grain sizes are greater than 11.09 nm, it considerately decreases when the grain sizes considerably continue declining. In addition, the UTS is the largest at d equals 11.09. The magnitude of UTS covers a wide range from 2.6 GPa to 3.015 GPa as the number of grains varies from 5 to 30. The range of UTS magnitude is similar to results obtained from different aluminum alloys [10].

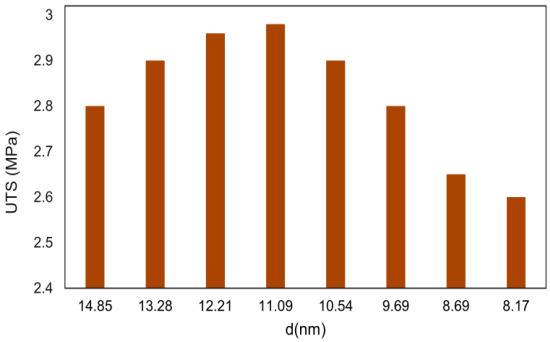

Fig. 3. The ultimate tensile stress of CGNMs with varying grain sizes.

The second important parameter is yield stress (YS) which decides whether the CGNMs are plastic deformation or only elastic behavior. The effect of grain size on YS can be shown using the inverse square root of grain diameter and the yield stress (YS), Hall – Petch's equation [13] determined the relation between the YS and $(d)^{1/2}$ following equation:

$$\sigma_{ys} = \sigma_0 + k_y d^{-\frac{1}{2}} \quad (GPa) \quad (5)$$

where σ_{ys} is the yield strength of the material, σ_0 is the initial stress of the material, k_y is a constant related to the crystal structure of the grain boundary, and d is the average diameter of the grain.

Based on the simulation results, the yield limit of materials with different grain sizes is determined. Applying the Hall - Petch equation, the graph of the relationship between yield stress and the square root of grain size is constructed as shown in Fig. 4.

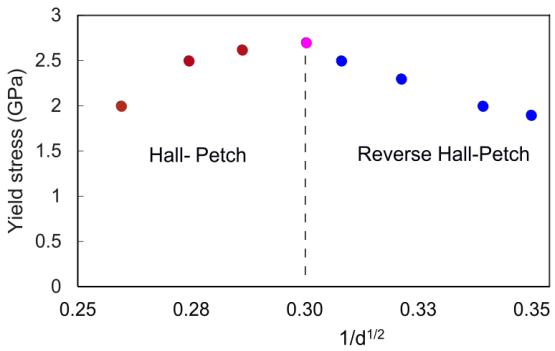

Fig. 4. Relation between yield stress and the inverse square root grain diameter

It is obvious that when $1/d^{1/2}$ $(nm)^{1/2}$ is smaller than 0.3, the YS of material CGNMs follows the Hall-Petch relation, if $1/d^{1/2}$ $(nm)^{1/2}$ is greater than 0.3 the reverse Hall-Petch relation is compatible.

The Hall-Petch relation was explained by slipping of dislocation. There is a limit to this mode of strengthening, as infinitely strong materials do not exist. When the grain size is large enough, the main mechanism for deformation is the movement of dislocation, where the grain boundary will restrict the movement of dislocation. When grain size increases, the distance between grain boundaries decreases, hence the free mean path of dislocation decreases, which increases the ultimate tensile strength. Grain sizes might range from about 100 μm (large grains) to 1 μm (small grains). Lower than this, the size of dislocations begins to approach the size of the grains. At a grain size of about 10 nm, only one or two dislocations can fit inside a grain. This scheme prohibits dislocation pile-up and instead results in grain boundary diffusion. The lattice resolves the applied stress by grain boundary sliding, decreasing the material's yield strength.

The grain size equals 11.09 nm, and the inverse Hall–Petch was observed. This is because when the grain size decreases at nm scale, there is an increase in the density of grain boundary junctions which serves as a source of crack growth or weak bonding. This is due to a decrease in the stress concentration of grain boundary junctions. These results are compatible with Chen *et al* [14] who have researched the inverse HallPetch relations of high-entropy alloys. In their work, polycrystalline models of FCC-structured $CoNiFeAl_{0.3}Cu_{0.7}$ with grain sizes ranging from 7.2 nm to 18.8 nm were constructed to perform uniaxial compression using molecular dynamic simulations. All compression simulations were done after setting the periodic boundary conditions across the three orthogonal directions. It was found that when the grain size is below 12.1 nm the inverse Hall–Petch relation was observed. This is because as the grain size decreases partial dislocations become less prominent and so does deformation twinning. Instead, it was observed that there is a change in the grain orientation and migration of grain boundaries thus causing the growth and shrinkage of neighboring grains. These are the mechanisms for inverse Hall–Petch relations. When the grain size is small enough, other mechanisms for plastic deformation will occur, such as grain boundary sliding. This new mechanism is favorable when decreasing the grain size, which explains the inverse Hall-Petch relation.

We can conclude that when decreasing grain size, the material will first follow the Hall-Petch relation, but then switch to the inverse Hall-Petch relation at a grain diameter smaller than 11.09 nm.

3.2. Microstructure Evolution of Compositionally Graded Nanowires

The mechanical behaviors of FCC materials have indicated the presence of various planar defects during tension, encompassing intrinsic stacking fault (ISF), extrinsic stacking fault (ESF), twin boundary (TB), and hexagonal close-packed (HCP) phase. The fraction of intrinsic stacking fault (ISF), extrinsic stacking fault (ESF), twin boundary (TB), and hexagonal close-packed (HCP) phase are present in Fig. 5.

These planar defects have previously been referred to as HCP structures. The formation of the HCP phase in an FCC crystal was analyzed using CNA first. However, there has been a lack of quantitative consideration for the individual contributions of each planar defect type in previous studies, despite their significance in understanding the plastic mechanisms of metallic materials.

Recently, S. Shuang *et al*. [15] introduced a novel and robust planar defect analysis (PDA) algorithm to classify various planar defects based on the nearest neighbor structures. This classification approach considers the coordinates of 12 atoms in the nearest neighbor to discern the atomic structures and planar defects. Additionally, the PDA compares the nearest neighbor structure of coordinating atoms for defect atoms with similar structural environments to capture the differences and effectively characterize local structures of planar defects. The PDA algorithm offers a quantitative assessment of the evolution of planar defects, thereby enhancing our understanding of the dynamics of planar defects within the material. In this study, we utilized the PDA algorithm to examine the configuration of atomic evolution of CuNi CGNMs.

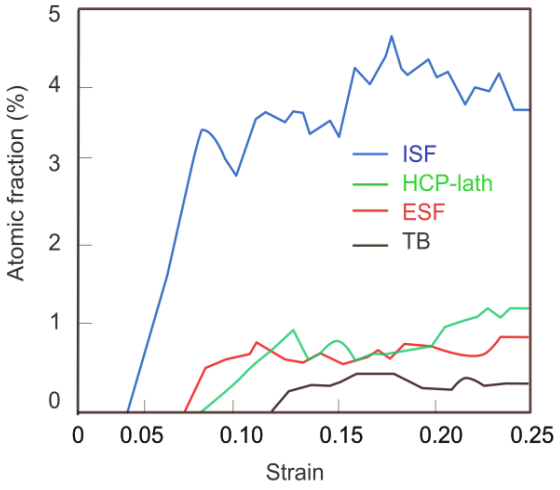

Fig. 5. Planar defect fraction of CuNi CGNMs with 12 grains.

The atomic configuration with planar defect configuration at strains of 0, 0.10, and 0.20 are present in Fig. 6.

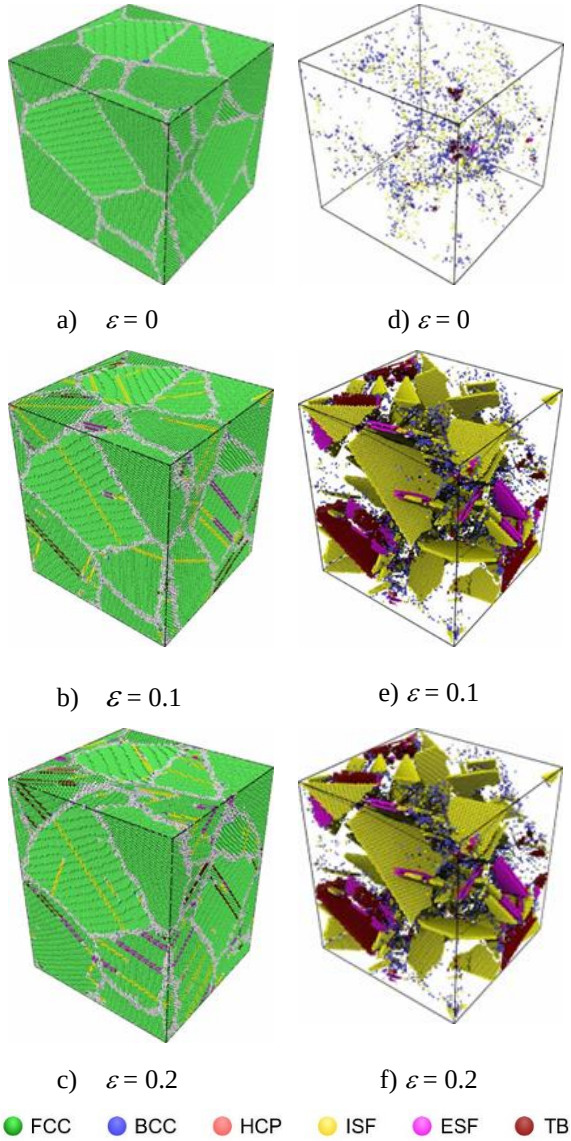

Fig. 6. Atomic configuration with (PDA) at strain at 0, 0.10, 0.20 (a-c). Planar defects configuration at strain at 0, 0.10, 0.20 (d-f), respectively

At the strain of 0, the defects do not exist in the materials, as shown in Fig. 6d. The range strain from 0.02 to 0.25, the material enters the plastic region, in which ISF increases substantially. The ISF increases due to crystal slipping, mostly in {111} direction, as shown in Fig. 6(e-f). After that, ISF only increases gradually. ESF also increases around 0.05 strain after ISF reaches its limit. ESF is also in {111} direction caused by crystal slipping, shown in Fig. 6 (e-f). The twinning mechanism also occurs at 0.07 strain, when the slipping mechanism becomes difficult. The twin boundaries are shown in Fig. 6 (e-f), but their quantity is lower than ISF and ESF (slipping).

The dominance of ISF defects and their varying trends with strain elucidate the intricate role of planar defects in influencing the mechanical behaviors of CGNMs. The behavior of ESF defects plays a crucial role, especially in CGNMs with higher defect densities. This could point towards different mechanical strengthening or weakening mechanisms activated under varying conditions. On the other hand, A few previous investigations have recently elucidated the softening mechanisms in single crystalline high entropy alloys (HEAs) and revealed a pronounced softening behavior in HEAs oriented in the [100] direction. Notably, a phase transition has been identified as the cause of this strain softening, contributing to the high flexibility observed in CGNMs. Therefore, the findings regarding phase-transition induced.

The strain softening in CGNMs from the present study aligns with those reported previously. Understanding these defect dynamics is crucial for tailoring material properties, optimizing structural performance, and advancing the design of high-performance materials with engineered nanostructures. Developing mathematical relations between the microstructure and mechanical properties would be beneficial as they directly link them. However, the establishment of mathematical quantitative ties faces considerable challenges due to the complex and dynamic nature of atomic configurations during deformation. The microstructure changes involve intricate and multifaceted interactions, making precise mathematical characterization particularly challenging. The dynamic nature of these configurations adds a significant obstacle in quantitatively correlating them with mechanical properties. Therefore, establishing direct mathematical relations between dynamic microstructural configurations and mechanical properties remains a complex area that requires further exploration and understanding

It can be concluded that the main mechanism of plastic deformation is crystal slipping (ISF with ESF) following twinning (twin boundary). The dominant planar defect is ISF.

3.3. Evolution of Dislocations

To gain deeper insights into the mechanical behaviors, the distributions of dislocations in CuNi PCGNMs (9 grains) were depicted in Fig. 7. The dislocation distributions are analyzed using dislocation analysis (DXA) in Ovito software, which reveals six types of dislocations: Perfect dislocation (Burgers vector: 1/2 <110>), Shockley partial dislocation (Burgers vector: 1/6 <112>), Stair-rod partial dislocation (Burgers vector: 1/6 <110>), Hirth partial dislocation (Burgers vector: 1/3 <100>), Frank partial dislocation (Burgers vector: 1/3 <111>) and other types of dislocation.

The dislocation segments are color-coded based on their types, as shown in Fig. 7. For the grain size with d = 11.09, all the partial dislocations are emitted at a strain of approximately 0, predominantly from the grain boundaries. This suggests that the grain boundaries act as many sources of dislocations for the deformation process. With the strain increasing to 0.1, the Shockley partial dislocation increases, while Stair-rod partial and other dislocations form and propagate. A few perfect dislocations, Hirth and Frank partial dislocations emerge at higher strain. Furthermore, all kinds of dislocations emit and propagate in the grain boundaries.

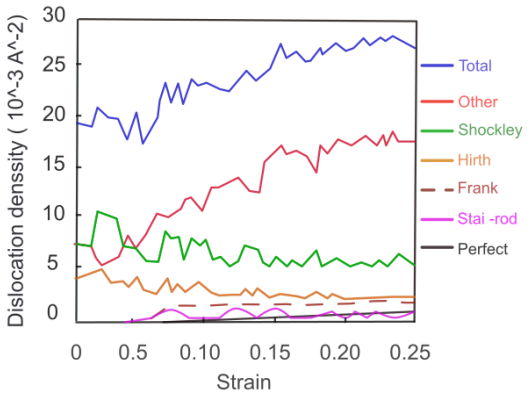

Fig. 7. The dislocation density of d equals 11.09

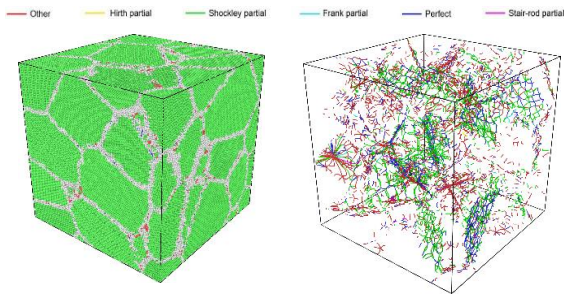

a) n = 18 (d = 9.69 nm)

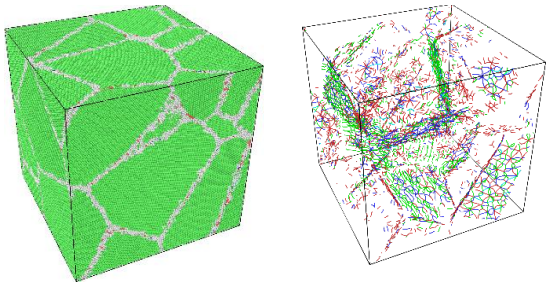

b) n = 7 (d = 13.28 nm)

Fig. 8. The dislocation cell on the grain boundaries at the strain equals 0,

To study the role of grain size on the mechanical behavior of the material, two simulation boxes with grain numbers n =18 (d = 9.69 nm) and n = 7 (d = 13.28 nm) are taken for analysis. The perfect dislocations and partial dislocations are presented in different colors in Fig. 8, Initially, when no tensile load is applied to the simulation box, the dislocations form as cells on the boundary. It can be seen that the grain boundaries act as the wall to prevent the dislocations from moving. In addition, the number and the dislocation density in both cases are similar as depicted in Fig. 8a, and Fig. 8b.

Originally, the others and Shockley dislocations were major. These dislocations are formed right from the moment of material fabrication, during the casting, crystallization, and solidification processes. They form dislocation cells located on grain boundaries and phase boundaries.

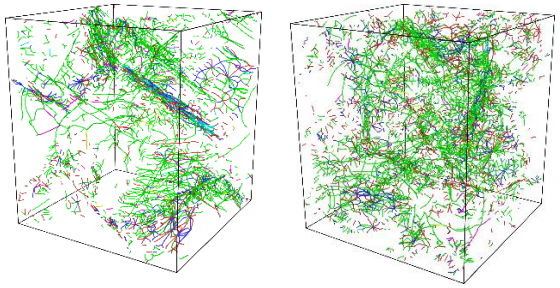

a) n = 7 (d =13.28 nm) b) n = 18 (d = 9.69 nm)

Fig. 9. Dislocation segments at strain at 0.125

It can be seen that there is already some dislocation in the materials at the strain of 0.125. These dislocations exist because of the grain boundary barrier. The dislocation density increases gradually as the strain increases. The only significant increase is the Shockley dislocation, which implies that Shockley partial dislocation with a planar defect is the main mechanism of plastic deformation. We can see Shockley dislocation at the center of the grain when plastically deformed, shown in Fig. 9 a and Fig. 9 b.

In the middle of the plastic deformation process, the Shockley dislocations increase significantly in both grain sizes. However, these dislocations with d is smaller than 11.09 nm are located on the grain boundaries Fig. 9a, and with d is greater than 11.09 nm these dislocations slip in the volume of the simulation box Fig. 9b. It can be seen that the dislocation density in two different grain sizes is not the same. The number of concentrated dislocations on the grain boundaries for the case of grain number equals 7 (d is smaller than 11.09 nm) is obvious in Fig. 9a. While a particle

number of 18 (d is greater than 11.09 nm), the grain size is too small, and does not have enough space to accommodate the dislocations. Therefore, the dislocations slide across the boundary very quickly in Fig. 9b. This phenomenon causes the changing properties of materials.

3.4. Microstructure Evolution of CGNMs

The mechanical and failure behaviors of CGNMs are investigated using molecular dynamic simulations, revealing a significant dependence on the grain size. Specifically, YM, UTS, and YS of CGNMs increased significantly for d less than or equal to 11.09 nm but rapidly decreased for d greater than 11.09 nm. The crystal structures of CGNMs under tension evolve from face center cubic (FCC) to body center cubic (BCC), and hexagon close-packed (HCP) transformations during plastic deformation processes, regardless of grain sizes.

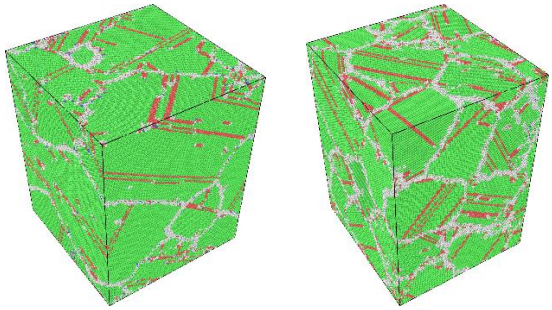

a) n = 7 (d =13.28 nm) b) n = 18 (d = 9.69 nm)

Fig. 10. The twinning at strain of 0.125

When tensile loads are applied to the material, crystal structure changes can occur at all grain sizes. However, the level of change is different in different grain sizes. The smaller the grain size, the greater the level of change in the milled network structure. The phenomenon of twinning appears from the boundaries. This can be seen through the evidence in Fig. 10. The proportion of twinning in n equals 7 (d = 13.28 nm) is less than the twinning ratio of n is equal to 18 (d = 9.69 nm). The stress required to form mechanical symmetry is usually greater than the stress needed to cause slippage. Therefore, the sliding of dislocations will occur first, and then the twin phenomenon of dislocations will form when sliding processes encounter difficulties.

6. Conclusion

The mechanical properties of CGNMs are investigated using molecular dynamic simulations, revealing a significant dependence on the composition of grain sizes. The main conclusions are obtained as follows:

1) When the average diameter of a grain d is greater than approximately 11.09 nm (critical grain size), the yield stress increases which shows the Hall-Petch relation. The flow stress decreases as the average diameter of grain d is smaller than 11.09 nm, which shows the inverse Hall-Petch effect.

2) For simulation boxes with an average diameter greater than 11.09 nm, dislocations accumulate on grain boundaries, forming dislocation walls that impede the movement of other dislocations, which causes material hardening and increases yield stress. On the contrary, the simulation boxes with an average diameter smaller than 11.09 nm. Since the grain volume is too small to contain dislocations, dislocations slide across grain boundaries easily, reducing the yield strength of the material.

3) The microstructural characterization corroborates with any the average diameter of grain *(d)*. The deformation is driven by dislocation gliding and stress-induced phase transformation from FCC to BCC, and HCP phases.

Acknowledgment

Vietnam Ministry of Education and Training funds this research under project number B2023-BKA-02.

Reference

[1] Shanmugavel P *et al.*, An overview of fracture analysis in functionally graded materials. Eur J Sci Res, vol. 68, pp. 412–419, 2012.

[2] F.Z. Zaoui *et al.*, New 2D and quasi-3D shear deformation theories for free vibration of functionally graded plates on elastic foundations, Composites Part B: Engineering, vol. 159, pp. 231–247, Feb. 2019. https://doi.org/10.1016/j.compositesb.2018.09.051

[3] P. Liu *et al.*, Buckling of stomatopod-dactyl-club-inspired functional gradient plates: A numerical study, Composite Structures, vol. 207, pp. 801-815, Jan. 2019. https://doi.org/10.1016/j.compstruct.2018.09.078

[4] Song M *et al.*, Bending and buckling analyses of functionally graded polymer composite plates reinforced with graphene nanoplatelets, Composites Part B: Engineering, vol. 134, pp. 106–113, Feb. 2018. https://doi.org/10.1016/j.compositesb.2017.09.043

[5] M. Islam *et al.*, Mechanical and vibrational characteristics of functionally graded Cu–Ni nanowire: a molecular dynamics study, Composites Part B: Eng, vol. 198, pp. 108212, Oct. 2020. https://doi.org/10.1016/j.compositesb.2020.108212

[6] M.-T. Le *et al.*, Prediction of tunable magnetoelectric properties in compositionally graded ferroelectric/ferromagnetic laminate nanocomposites, Applied Physics Letters, vol. 118, pp. 052905, Feb. 2021. https://doi.org/10.1063/5.0041703

[7] L. V. Lich *et al.,* Abnormal Electromechanical Property of Nonlinearly Graded Lead-Free Ferroelectric Thin Films, Advanced Theory and Simulations, vol. 5, iss. 2, 2100370, Feb. 2022. https://doi.org/10.1002/adts.202100370

[8] Z. Yin *et al.,* Hybrid Catalyst Coupling Single-Atom Ni and Nanoscale Cu for Efficient CO_2 Electroreduction to Ethylene. J. Am. Chem. Soc. 144, pp. 20931–20938, 2022. https://doi.org/10.1021/jacs.2c09773

[9] M.M. Shahzamanian *et al.,* Analysis of stress shielding reduction in bone fracture fixation implant using functionally graded materials, Compos. Struct., vol. 321, 117262, 2023. https://doi.org/10.1016/j.compstruct.2023.117262

[10] M.A. Eltaher *et al.,* Predictive model for indentation of elastoplastic functionally graded composites, Compos. B: Eng, vol. 197, 108129, 2022. https://doi.org/10.1016/j.compositesb.2020.108129

[11] C. Cui *et al.,* Molecular dynamics study on tensile strength of twist grain boundary structures under uniaxial tension in copper, Vacuum 184, 109924, 2021. https://doi.org/10.1016/j.vacuum.2020.109874

[12] D. D. D. Ma *et al.,* Small-diameter silicon nanowire surfaces, Science 299, 2023, 1874. https://doi.org/10.1126/science.1080313

[13] E. O. Hall *et al.,* The deformation and aging of mild steel III. Discussion of results, Proceedings of the Physical Society B, 64, pp. 747, 1951. https://doi.org/10.1088/0370-1301/64/9/303

[14] Chen, Shuai, *et al.* Hall-Petch and inverse Hall-Petch relations in high-entropy CoNiFeAlxCu1-x alloys. Materials Science and Engineering: A 773, 138873, 2020. https://doi.org/10.1016/j.msea.2019.138873

[15] S. Shuang *et al.,* Effect of loading orientation on plasticity in the nano-laminated dual-phase high-entropy alloy: a molecular dynamics study, Modelling and Simulation in Materials Science and Engineering, vol. 31, no. 1, 015005, Dec. 2022. https://doi.org/10.1088/1361-651X/aca4ed